International Journal of Solids and Structures 50 (2013) 2798–2807

Contents lists available at SciVerse ScienceDirect

International Journal of Solids and Structures

journal homepage: www.elsevier.com/locate/ijsolstr

Symbolic and numerical solution of the axisymmetric indentation problem for a multilayered elastic coating

A. Constantinescu [a], A.M. Korsunsky [b], O. Pison [a], A. Oueslati [c,*]

[a] Laboratoire de Mécanique des Solides, CNRS UMR 7649– Ecole Polytechnique, 91128 Palaiseau cedex, France
[b] Department of Engineering Science, University of Oxford, Parks Road, Oxford OX1 3PJ, England, United Kingdom
[c] Université de Lille 1, UFR de Mathématiques, Laboratoire de Mécanique de Lille/CNRS UMR 8107, 59655 Villeneuve d'Ascq, France

ARTICLE INFO

Article history:
Received 5 September 2012
Received in revised form 18 March 2013
Available online 3 May 2013

Keywords:
Indentation
Multilayer
Transfer matrix
Integral equation
Mathematica

ABSTRACT

This paper is concerned with a semi-analytical approach to the solution of the axisymmetric indentation problem for a multilayered elastic half-space. The stress and displacement fields for each layer and the substrate are derived in closed form by using the Papkovich–Neuber potentials and the Hankel transform. The bonded or sliding interface conditions between the sub-layers are handled by the use of the appropriate transfer matrix, and then the mixed boundary value problem is reduced to a Fredholm integral equation. Symbolic and numerical computations of the solution are implemented in the symbolic software Mathematica in the form of a fast and efficient numerical algorithm, allowing rapid determination of the load–displacement curves and composite elastic properties for an arbitrary rigid indenter shape. A series of results for different indenters (flat, conical, spherical and blunted conical punch shapes) and different multilayered composites is presented and discussed.

The complete set of symbolic and numerical computations are provided as supplementary resources with the paper.

1. Introduction

Thin films and surface coatings are of a great importance in the context of many engineering applications, e.g. for the improvement of resistance to wear, increasing the strength and toughness of structural surfaces and the protection of solids in high temperature or corrosive environments. Multilayered or continuously graded materials offer the potential for further progress in optimized design of surface coatings. For the purpose of design optimization, the knowledge of properties of such materials is crucial. Undoubtedly, indentation is the approach most widely used for the identification of thin film properties spanning the range of scales from nanometer to macroscopic. The evaluation procedure is based on the analysis of the indentation curve P–h representing the applied load P on the indenter with respect to its penetration depth h during the loading/unloading test. The simplest approach to the problem would be to find suitable laws that describe some parts of the indentation curve, and then to extract the material properties as fitting parameters. However, even in the presence of such analytical descriptions, the identification of material properties through indentation analysis is a difficult inverse problem. As in most cases of inverse analysis, the direct problem has to be addressed first.

The standard method used in the direct approach to evaluating Young's modulus of a homogeneous bulk substrate was initially developed by Oliver and Pharr (1992) and improved later in Oliver and Pharr (2004). They proposed a relationship between the initial unloading slope of the P–h curve and the substrate's Young's modulus. The remaining parameters were obtained by a Finite Elements Analysis (FEA). Using the Oliver and Pharr framework, Dao et al. (2001) found a complete set of explicit analytical functions using dimensional analysis and then FEA. Those functions help solving the direct problem, i.e. finding the parameters that describe the loading/unloading slopes of the indentation curve. Also, these functions can be used for the inverse analysis of the indentation test. These procedures have been extended for extracting materials properties of anisotropic solids (Delafargue and Ulm, 2004; Vlassak and Nix, 1994; Swadener and Pharr, 2001; Vlassak et al., 2003).

For heterogeneous materials, some analytical solutions can be found in literature. Giannakopoulos and Suresh (1997a,b) developed solutions for several indenter tips under the assumption that the depth distribution of the substrate's Young's modulus follows a power law or exponential law. Then Choi et al. (2008a,b) extended this approach to plastically graded materials using a similar approach to that of Dao et al. (2001). Nevertheless, often no a priori assumption can be made regarding the depth distribution of properties, and hence a multi-layer approach is necessary. Ke and Wang (2006) developed semi-analytical solutions for the plane strain problem using linear piecewise property distributions in each

* Corresponding author. Tel.: +33 3 20 33 71 71; fax: +33 3 20 33 71 53.
E-mail address: abdelbacet.oueslati@univ-lille1.fr (A. Oueslati).

0020-7683/$ - see front matter © 2013 Elsevier Ltd. All rights reserved.
http://dx.doi.org/10.1016/j.ijsolstr.2013.04.017

layer. However, the indentation problem is most often approximated as axisymmetric. For such problems some solutions have also been documented in the literature, e.g. the elastic solution of a homogenous layered half space with perfect interfacial bonding under axisymmetrical compressive loading carried out by Li and Chou (1997). Due to the complexity of the integrals involved in the use of the Hankel transform, the elastic fields for the coating/substrate system were obtained by a numerical inversion procedure. A different method of solution for the indentation of a thin film deposited on an elastic substrate and indented by an axisymmetric rigid punch was presented by Yu et al. (1990). This approach used the method proposed by Lebedev and Uflyand (1958) which results in the formulation of a Fredholm integral equation. The merit of this method of analysis lies in its ease of numerical implementation and the possibility of its application to a large range of different indenter tips. Fretigny and Chateauminois (2007) studied the problem with a constant piecewise distribution of elastic parameters by adopting a matrix formalism. They investigated the case of one layer over a substrate, but gave directions on how to generalize the method of solution to multilayered solids. Tang et al. (2008, 2009) studied experimentally and numerically the elastic modulus of metal-ceramic nanolaminates measured by axisymmetric nanoindentation. The elastic modulus of the multilayer was obtained according to the method proposed by Oliver and Pharr (1992). Recently, Korsunsky and Constantinescu (2009) used the technique of Yu et al. (1990) in order to study the influence of punch tip sharpness on the interpretation of indentation measurements for the layered elastic half-space. Perfectly bonded or freely sliding boundary conditions between the film and the substrate were taken into account. The authors considered axisymmetric indenters with different tip shapes, namely, the flat punch, spherical indenter, as well as conical and blunted conical indenters.

In this work, we consider the frictionless axisymmetric indentation of a multilayer lying on a semi-infinite elastic substrate. This problem can be seen as the indentation of an elastically graded material with constant piecewise distributions. Extending Korsunsky and Constantinescu's (2009) approach for a single layer to an arbitrary number of layers on a dissimilar substrate, we present a symbolic/numerical method of solution of the direct problem for several rigid indenter shapes. The use of symbolic computation permits several goals to be achieved, namely: (i) to verify the accuracy of the closed form solutions and to eliminate coding errors, (ii) to create a numerical code that performs the computation for n layers, where the number n is not predefined. Compared to the Finite Element Method, this approach is not limited by the size of elements that represent the thickness of the layers, and a better parametric understanding of the deformation phenomena during indentation becomes possible.

2. The multilayer coating indentation problem

Let us consider a multilayer composed of n layers deposited upon a half-space and being indented by an axisymmetric rigid punch as shown in Fig. 1. Both the layers and and the half-space are assumed to be homogeneous with a linear isotropic elastic behavior. The layers are indexed by $i = 1, n$ with increasing depth, each characterized by thickness h_i, shear modulus μ_i and Poisson's ratio ν_i.

For the rigid, axially symmetric indenter, four different shapes are considered next: the flat punch, the spherical cap, the sharp conical indenter and the blunted conical indenter (see sketches in Fig. 2).

The contact is considered to be frictionless and the problem is treated under the assumption of small strains. Cylindrical coordinates (r, θ, z) are used, with $z > 0$ pointing into the substrate, and each problem posed in terms of (i) the elasticity equations for each layer and the half space, (ii) the boundary conditions between layers, and (iii) the contact boundary conditions between the indenter and the first layer.

The elastic displacement and stress fields will be expressed in terms of the Papkovich–Neuber displacement potentials, given by the harmonic vector and the scalar function $\underline{\Psi^j} = \left(0, 0, \Psi^j\right)$ and ϕ^j respectively. (For a complete presentation of the Papkovich–Neuber potentials see, for example (Constantinescu and Korsunsky, 2007; Robert and W., 1999; Solomon, 1968)). The harmonicity of the potentials insures that the equations of linear isotropic elasticity are satisfied in each layer.

The elastic displacement and stress fields are given by:

$$2\mu_j u_r^j = -\phi_{,r}^j - z\psi_{,r}^j \tag{1}$$

$$2\mu_j u_z^j = k_j\psi^j - \phi_{,z}^j - z\psi_{,z}^j \tag{2}$$

$$\sigma_{zz}^j = 2(1-\nu_j)\psi_{,z}^j - \phi_{,zz}^j - z\psi_{,zz}^j \tag{3}$$

$$\sigma_{rz}^j = (1-2\nu_j)\psi_{,r}^j - \phi_{,rz}^j - z\psi_{,rz}^j \tag{4}$$

where $\kappa_j = 3 - 4\nu_j, u_r^j, u_z^j$ denote the components of the displacement vector, $\sigma_{zz}^j, \sigma_{rz}^j$ are the components of the stress tensor and the superscript j denotes the number of layer, and refer to the substrate if $j = n+1$.

Under the assumption of axial symmetry, the harmonic potentials ψ^i and ϕ^i can be expressed as the Hankel transform of four unknown arbitrary functions (Yu et al., 1990) $A_1^i(\lambda), A_2^i(\lambda), A_3^i(\lambda), A_4^i(\lambda)$.

The potentials in each layer i, for $(r,z) \in [0, +\infty[\times[z_{i-1}, z_i]$, are given by:

$$\psi^i(r,z) = \int_0^\infty \left(A_1^i \cosh(\lambda(z - z_{i-1}) + A_2^i \sinh(\lambda(z - z_{i-1}))\right) \times \frac{J_0(\lambda r)}{\sinh(\lambda(z_i - z_{i-1}))}\, d\lambda \tag{5}$$

$$\phi^i(r,z) = \int_0^\infty \left(A_4^i \cosh(\lambda(z - z_{i-1})) + A_3^i \sinh(\lambda(z - z_{i-1}))\right) \times \frac{J_0(\lambda r)}{\lambda \sinh(\lambda(z_i - z_{i-1}))}\, d\lambda \tag{6}$$

where $\sinh()$ and $\cosh()$ are the hyperbolic sine and cosine functions and J_0 is the Bessel function of first kind of order zero.

For the substrate, the expressions for the potentials are:

$$\psi^{n+1}(r,z) = \int_0^\infty A_5(\lambda)\exp(-\lambda(z - z_n))J_0(\lambda r)\, d\lambda \tag{7}$$

$$\varphi^{n+1}(r,z) = \int_0^\infty A_6(\lambda)\exp(-\lambda(z - z_n))\frac{J_0(\lambda r)}{\lambda}\, d\lambda \tag{8}$$

It may be seen that the expressions for the potentials in (6)–(8) ensure that stresses and their derivatives vanish in the layers for $z > 0$ if $r \to \infty$ and in the substrate for $r > 0$ if $z \to \infty$.

The boundary conditions between two successive layers i and $i+1$ are described either as a *perfect bonding* or as *frictionless sliding*.

Perfectly bonded layers impose the continuity of displacements and surface tractions (hence continuity of stress components zz and rz) at the respective interface:

$$u_z^i(r,h) = u_z^{i+1}(r,h) \tag{9}$$

$$u_r^i(r,h) = u_r^{i+1}(r,h) \tag{10}$$

$$\sigma_{zz}^i(r,h) = \sigma_{zz}^{i+1}(r,h) \tag{11}$$

$$\sigma_{rz}^i(r,h) = \sigma_{rz}^{i+1}(r,h) \tag{12}$$

Frictionless sliding between layers imposes the continuity of normal components of displacement and surface tractions and the vanishing of tangential surface traction:

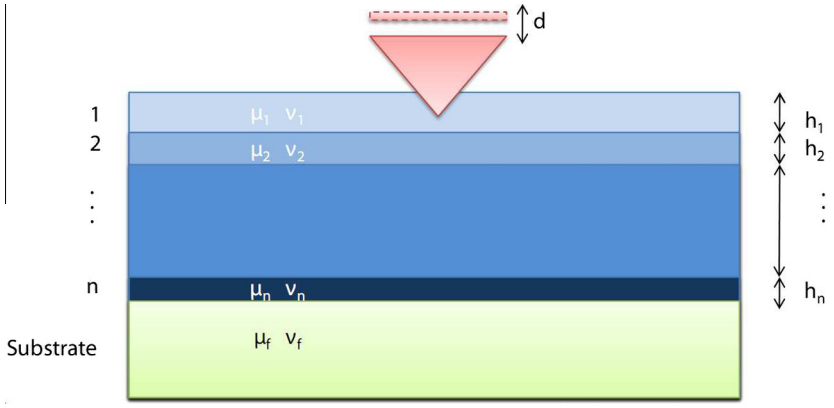

Fig. 1. Indentation of a multilayer.

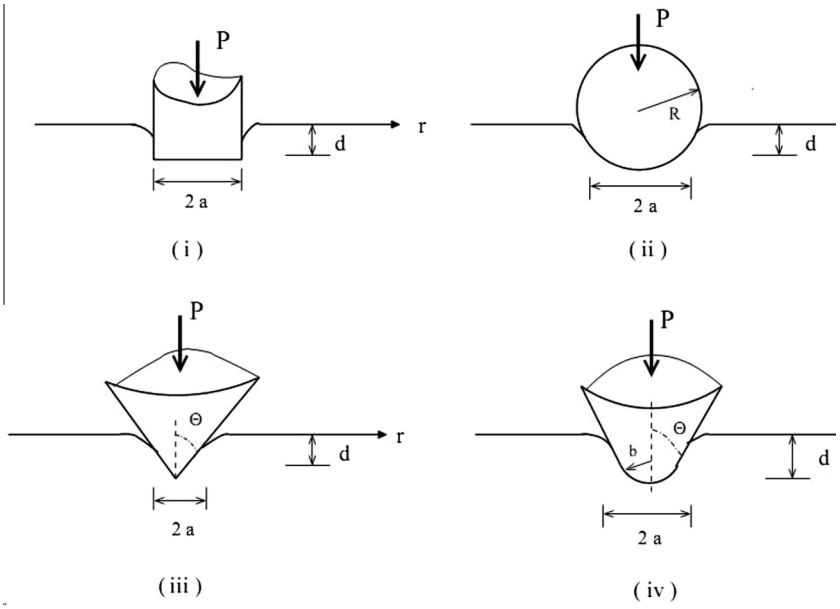

Fig. 2. Axisymmetric Indenters: (i) flat punch, (ii) spherical cap, (iii) conical indenter and (iv) blunted conical indenter.

$$u_z^i(r,h) = u_z^{i+1}(r,h) \tag{13}$$
$$\sigma_{zz}^i(r,h) = \sigma_{zz}^{i+1}(r,h) \tag{14}$$
$$\sigma_{rz}^i(r,h) = \sigma_{rz}^{i+1}(r,h) = 0 \tag{15}$$

The boundary conditions for the upper surface $z = 0$ express: (a) the traction-free surface for $a \leqslant r \leqslant \infty$, (b) the frictionless contact between the rigid indenter and the first layer, and (c) the fact that the tangential component of the surface traction is zero everywhere. These conditions are given by:

$$u_z^1(r,0) = d - \delta(r) \quad (0 \leqslant r \leqslant a) \tag{16}$$
$$\sigma_{zz}^1(r,0) = 0 \quad (a \leqslant r \leqslant \infty) \tag{17}$$
$$\sigma_{rz}^1(r,0) = 0 \quad (0 \leqslant r \leqslant \infty) \tag{18}$$

where d denotes the penetration depth, $\delta(r)$ the indenter shape and a is the radius of contact.

The corresponding symbolic computations in Mathematica (Wolfram. S) of the preceding equations and their deduction are provided in the supplementary resources provided with the paper (see file `TransferMatrix.nb`).

3. Method of solution

The solution of the indentation problem in terms of the Papkovich–Neuber potentials (and hence elastic displacements and stress fields) requires the determination of the $4n+2$ unknown functions: $A_1^i(\lambda), A_2^i(\lambda), A_3^i(\lambda), A_4^i(\lambda)$ $i = 1, n$ for the layers and $A_5(\lambda)$ and $A_6(\lambda)$ for the substrate. The equations relating the unknown functions are only the interface conditions between the layers and the contact and free surface conditions at the upper surface of the multilayer.

The solution method relies on the three steps originally described in Yu et al. (1990): (i) the transformation of the contact Eq. (16) into two integral equations in terms of function $A_1^1(\lambda)$, the contact radius a and an auxiliary function $g(\lambda)$. The principal unknowns of the problem will be related to $A_1^1(\lambda)$. (ii) The construction of $g(\lambda)$ from the interface conditions between layers and (iii) the determination of $A_1^1(\lambda)$ as the solution of two integral equations defined in (i) using the method proposed by Lebedev and Uflyand (1958).

The contact boundary conditions (16) and (17) can be rewritten as the following set of integral equations

$$\int_0^\infty h(\lambda) J_0(\lambda r)\, d\lambda = f(r) \tag{19}$$

$$\int_0^\infty \frac{h(\lambda)}{1-g(\lambda)} \lambda J_0(\lambda r)\, d\lambda = 0 \tag{20}$$

where the following notations have been introduced

$$h(\lambda) = \frac{A_1^1(\lambda)}{\sinh(\lambda h_1)} \tag{21}$$

$$f(r) = \frac{\mu_1}{1-\nu_1}(d-\delta(r)) \tag{22}$$

$$g(\lambda) = 1 - \frac{A_1^1(\lambda)}{A_4^1(\lambda) - 2(1-\nu_1)A_2^1(\lambda)} \tag{23}$$

The condition of the tangential component of traction, Eq. (18), vanishing at the surface permits to establish the following equality:

$$A_3^1(\lambda) = (1-2\nu_1)A_1^1(\lambda) \tag{24}$$

so that A_3^1 can be eliminated.

Let us further denote by $\{A^i\}$ and $\{A^{n+1}\}$ the vector of unknown functions corresponding to layer i and to the substrate, respectively:

$$\left[A^i\right] = \left[A_1^i\, A_2^i\, A_3^i\, A_4^i\right]^T \quad i = 1, n \tag{25}$$

$$\left[A^{n+1}\right] = [A_5 A_6]^T \tag{26}$$

The symbolic algebraic computation of the displacements and stresses for different interface conditions shows that for both cases of sliding and perfectly bonded layers, the relationships between them take the form of linear expressions that can be condensed into the following matrix equations:

$$\left[A^i\right] = [\mathcal{I}_{i+1}]\left[A^{i+1}\right] \quad i = 1, n \tag{27}$$

$$\left[A^n\right] = [\mathcal{I}_{n+1}]\left[A^{n+1}\right] \tag{28}$$

Here $[\mathcal{I}_{i+1}]$ and $[\mathcal{I}_{n+1}]$ are the square (4 x 4) and the rectangular (4 x 2) transfer matrices that transmit the "elastic information" from one layer to the next. The coefficients of these matrices are rational functions formed by the combinations of $sinh(\lambda)$, $cosh(\lambda)$,$J_0(\lambda)$,... and the elastic moduli of the layers and their thickness. The expression of displacements and stresses conducting to the transfer matrices are computed symbolically in the supplementary Mathematica file `TransferMatrix.nb` provided with the paper. For a similar discussion of transfer matrixes in the elastic analysis of layered solids see for example (Bahar, 1972; Wang et al., 2002; Yue and Yin, 1998).

As a consequence, $\left[A^i\right]$, the unknown functions for layer i are related to the functions for the substrate $\left[A^{n+1}\right]$ by:

$$\left\{A^i\right\} = \prod_{k=i+1}^{n+1} [\mathcal{I}^k]\left[A^{n+1}\right]. \tag{29}$$

In particular, the functions for the surface layer $i = 1$ are given by:

$$\left\{A^1\right\} = \prod_{k=2}^{n+1} [\mathcal{I}^k]\left[A^{n+1}\right] \tag{30}$$

The interface conditions expressed in Eq. (30), together with the tangential traction-free condition at the surface (24) result in a system of five equations and six unknowns. It is easy to show that the system has a solution in terms of A_1^1, and that A_2^1 and A_4^1 are proportional to A_1^1. Therefore

$$g(\lambda) = 1 - \frac{A_1^1(\lambda)}{A_4^1(\lambda) - 2(1-\nu_1)A_2^1(\lambda)} \tag{31}$$

is a function that can be readily evaluated, as it depends only on the properties of the layers and the parameter λ.

In the case of a single layer over a substrate ($n = 1$), the explicit expression for g could be derived analytically. The expression was first given in Yu et al. (1990). Thanks to the availability of symbolic algebra packages, several errors were found in that expression, and were corrected in Korsunsky and Constantinescu (2009).

In the case of the multilayer coating discussed here ($n > 1$) it is still possible to perform the derivations analytically. However, due to the size and complexity of the expression sought, and the need to eliminate errors in the working, a symbolic algebra computer package was used for the derivation. This step has been split into three operations. (i) The expressions for the interface boundary conditions were obtained by symbolic manipulation of the Papkovich–Neuber potentials, and closed form expressions of $[\mathcal{I}^k]$ were computed. (ii) Taking the properties of the two layers surrounding each interface, expressions for matrices $[\mathcal{I}^k]$ were derived as a function λ. In preparation for numerical calculations, these matrix functions were stored in "compiled" form, meaning that derivation did not require repeating. (iii) The matrix product $\prod_{k=2}^{n+1}[\mathcal{I}^k]$ was computed. (iii) Finally, function g was defined as the solution of system (30).

The solution of the integral Eq. (20) was then constructed following the method of Lebedev and Uflyand (1958) and the procedure presented in Yu et al. (1990) and Korsunsky and Constantinescu (2009). The solution $h(\lambda) = A_1^1(\lambda)/\sinh(\lambda h_1)$ is sought in the form:

$$h(\lambda) = (1-g(\lambda))\int_0^a \phi(t)\cos\lambda t\, dt \tag{32}$$

which is equivalent to writing:

$$A_1^1(\lambda) = [1-g(\lambda)]\sinh(\lambda h_1)\int_0^a \frac{2\mu_1 d}{\pi(1-\nu_1)} H(t/a)\cos(\lambda t)dt \tag{33}$$

with the unknown function H related to ϕ by:

$$H(t/a) = \frac{\pi(1-\nu_1)}{2\mu_1 d}\phi(t) \tag{34}$$

According to the proof given in Lebedev and Uflyand (1958), H is the solution of the Fredholm equation of the second kind:

Table 1
Functions $\delta(r)$ and $F(\tau)$ for different shape indenters.

Indenter	$\delta(r)$	$F(\tau)$	E^*
Flat punch	0	0	$\frac{P}{2da}$
Spherical indenter	$\frac{r^2}{2R}$	$1-\frac{a^2\tau^2}{Rd}$	$\frac{3P}{4}\left(\frac{1}{Rd^3}\right)^{\frac{1}{2}}$
Cone	$r\,cot\theta$	$1-\frac{\pi}{2}\frac{a\tau}{d}cot\theta$	$\frac{\pi P}{2d^2}cot\theta$
Blunted conical indenter	$\begin{cases}\frac{r^2}{2R} & \text{if} r \leqslant b\\ \frac{b}{R}(R-\frac{b}{2}) & \text{if} r > b\end{cases}$	$\begin{cases}1-\frac{a^2\tau^2}{2R}cot\theta\\ -\frac{a^2\tau^2}{bd}cot\theta\left(1-\sqrt{1-\frac{b^2}{a^2\tau^2}}+\frac{b}{a\tau}arcos(\frac{b}{a\tau})\right)\end{cases}$	$\frac{\pi P}{2d^2}cot\theta$

$$H(\tau) - \frac{1}{\pi}\int_0^1 M(y,\tau)H(y)dy = F(\tau), \quad (0 \leqslant \tau \leqslant 1), \tag{35}$$

where $\tau = t/a \in [0,1]$ is the normalized radial coordinate within the contact circle. The right hand side F depends only on the total indentation depth and the indenter shape:

$$F(\tau) = 1 - \frac{a\tau}{d}\int_0^{\pi/2} \delta'(a\tau\sin\theta)\mathrm{d}\theta. \tag{36}$$

and the kernels $\mathcal{M}$ and K are given by Yu et al. (1990):

$$\mathcal{M}(y,\tau) = K(y+\tau) + K(y-\tau) \tag{37}$$

$$K(u) = \frac{a}{h_1}\int_0^\infty g\left(\frac{w}{h_1}\right)\cos\left(\frac{auw}{h_1}\right)\mathrm{d}w, \tag{38}$$

where h_1 denotes the thickness of the first layer. The kernel $\mathcal{M}(y,\tau)$ depends on the elastic properties and thickness of the layers and the substrate through the function g, and on the contact radius a. After some symbolic manipulations, the kernel $\mathcal{M}$ is expressed in the equivalent form:

$$M(y,\tau) = 2\frac{a}{h_1}\int_0^\infty g\left(\frac{w}{h_1}\right)\cos\left(\frac{ayw}{h_1}\right)\cos\left(\frac{a\tau w}{h_1}\right)\mathrm{d}w, \tag{39}$$

In order to streamline the computation of g for arbitrary values of its argument, it is best to define it as a compiled function in Mathematica. Then the kernels K and $\mathcal{M}$ need to be evaluated by integration over $[0,\infty]$. Two difficulties that arise concern the infinite integration interval and the highly oscillatory nature of the integrand. By examining the expression for K and through extensive numerical experiments for a wide range materials, we found that the thickness of the first layer h_1 appears to be the factor that determines the necessary range of integration, and that adequate estimates of g are obtained by integration over the interval $\left[0,\frac{5}{h_1}\right]$.

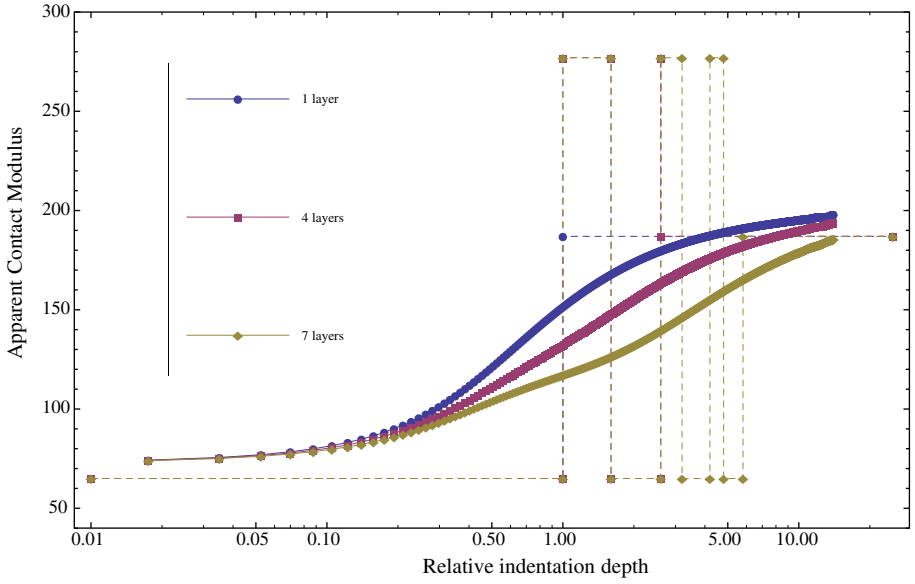

Fig. 3. The apparent contact modulus versus relative indentation depth for perfectly bonded multilayers composed of 1, 4 and 7 Al/SiC films indented by a cone.

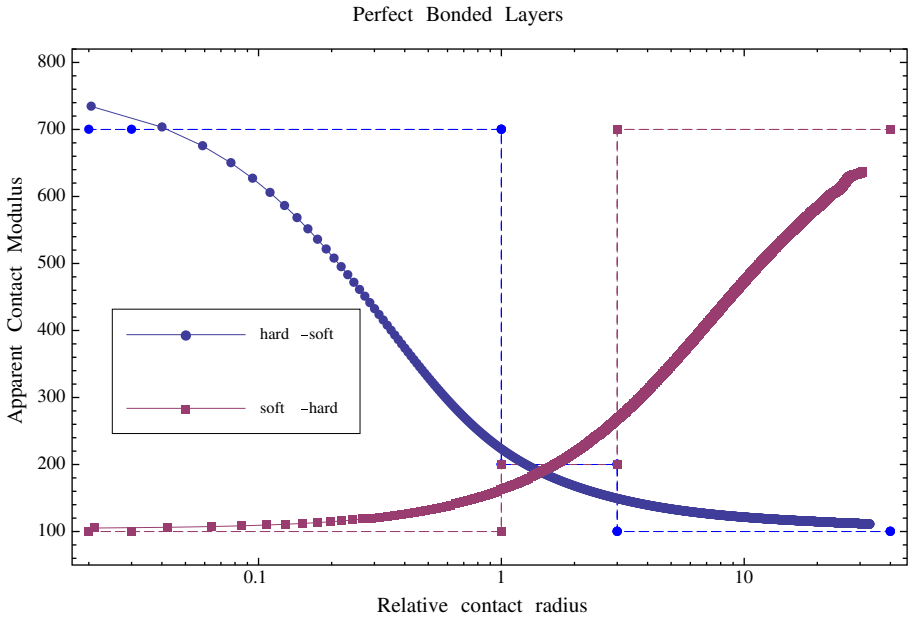

Fig. 4. The apparent contact modulus versus relative indentation depth for perfectly bonded bi-layer indented by a cone.

Several quadrature techniques were tested in order to sum correctly the oscillatory integrand. Namely, *Gauss–Legendre Quadrature*, *Fourier Cosine Transform* and the standard numerical integration operators in Mathematica were tested. We concluded that, with correct choice of the support of g, the *Gauss–Legendre Quadrature* provided the best trade-off between speed and accuracy.

The integral Eq. (35) H is solved using a *Gauss–Legendre* discretization that represents it as the linear system:

$$[\mathcal{M}^*].\{H\} = \{F\} \tag{40}$$

More precisely:

$$\mathcal{M}^*_{ij} = \delta_{ij} - \frac{1}{\pi}\left(w_i\left(K(x_i + x_j) + K(x_i - x_j)\right)\right) \tag{41}$$

$$\begin{cases} \{H\}_j = H(x_j) \\ \{F\}_j = F(x_j) \end{cases} \quad i,j = 1, n_g \tag{42}$$

where w_i denotes the weight assigned to the function value at the Gauss point x_i, and n_g is the number of Gauss points or equivalently the degree of the Legendre polynomial.

Thus, a solution H can be found from (35) for any value of a. However, a question about determining the contact radius a may remain outstanding. Two cases can be distinguished: either a is given and fixed, as e.g. in the case of a flat punch; or, as e.g. for a spherical cap, the value of a is unknown a priori. In this case, however, the condition of continuous variation of stresses at the layer surface can be imposed. The requirement that the surface tractions fall to zero at the edge of the contact zone is expressed as:

$$\sigma_{zz}(a, 0) = 0$$

From the expression for the stresses given in Lebedev and Uflyand (1958):

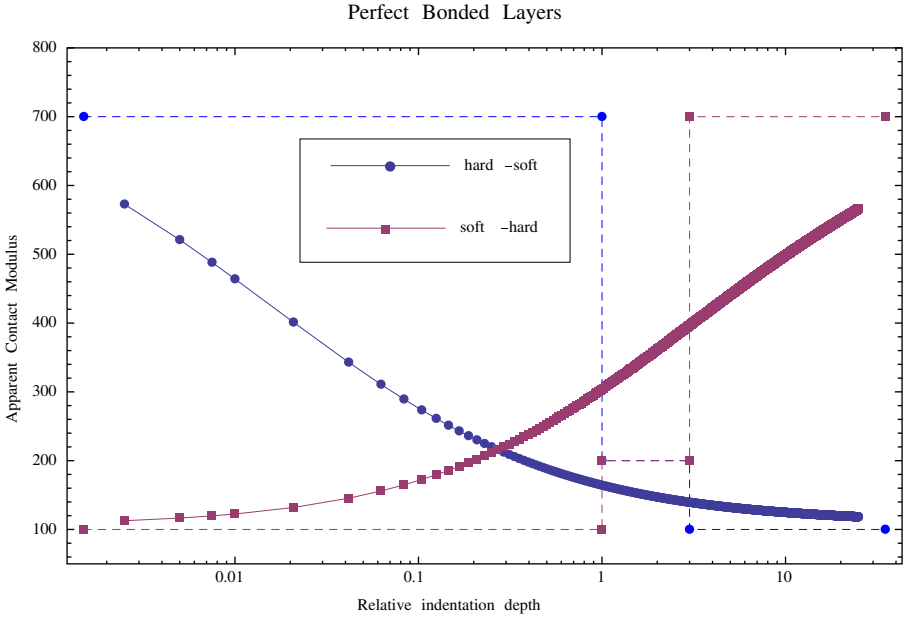

Fig. 5. The apparent contact modulus versus relative indentation depth for perfectly bonded bi-layer indented by a spherical cone.

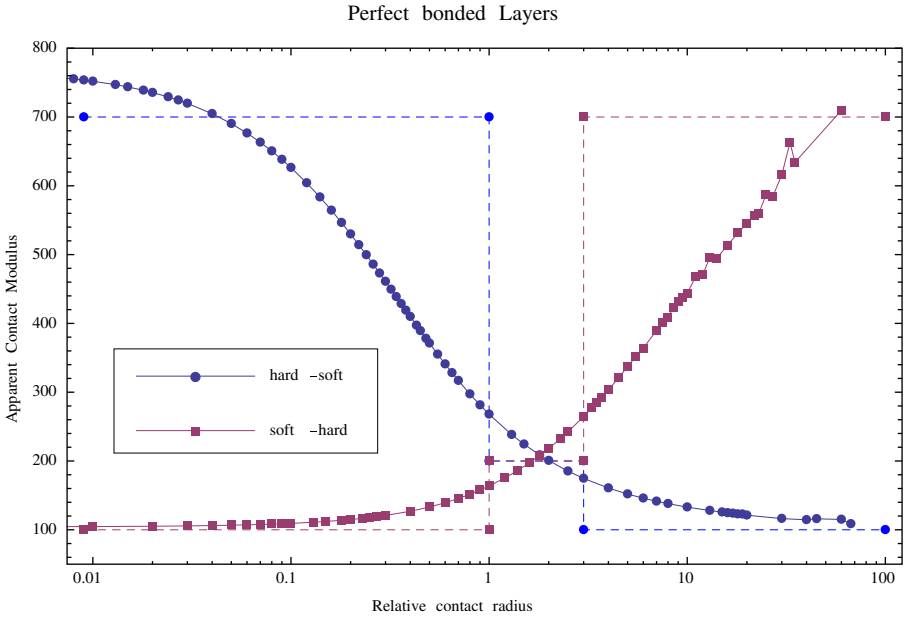

Fig. 6. The apparent contact modulus versus relative contact radius for perfectly bonded bi-layer indented by a flat punch.

$$\sigma_{zz}(r,0) = \int_r^a \frac{\phi'(t)}{\sqrt{t^2-r^2}}\,dt - \frac{\phi(a)}{\sqrt{a^2-r^2}} \text{ when } r < a. \tag{43}$$

where $\phi(x) = \sinh(\lambda h_1)\ \frac{2\mu_1 d}{\pi(1-\nu_1)} H(x/a)$, one can rewrite the continuity condition as:

$$\phi(a) = 0 \quad \text{or} \quad H(1) = 0 \tag{44}$$

For a given value of d function $H(a,d)$ appears to be a monotonic function of a. Therefore we employ dichotomy for numerical evaluation of the contact radius a.

The numerical algorithm performs the following iterative steps:

1. Select a trial value of the contact radius a;
2. Compute H as a function of a by solving the integral Eq. (35);
3. Check the continuity of normal surface traction at the edge of the contact circle, and correct the contact radius a.

The total indentation load is obtained by integrating the pressure distribution under the indenter, as given by

$$P = 4ad\frac{\mu_1}{1-\nu_1}\int_0^1 H(\tau)\mathrm{d}\tau. \tag{45}$$

Finally, let us define the apparent contact modulus for the coating system by:

$$E^* = \frac{P}{2da_H(d)}\left[\int_0^1 F(\tau)d\tau\right]^{-1} \tag{46}$$

where $a_H(d)$ denotes the contact radius as function of the displacement d for the homogenous substrate (for a series closed-form expressions for $a_H(d)$ for different indenter shapes see Korsunsky and Constantinescu (2009)).

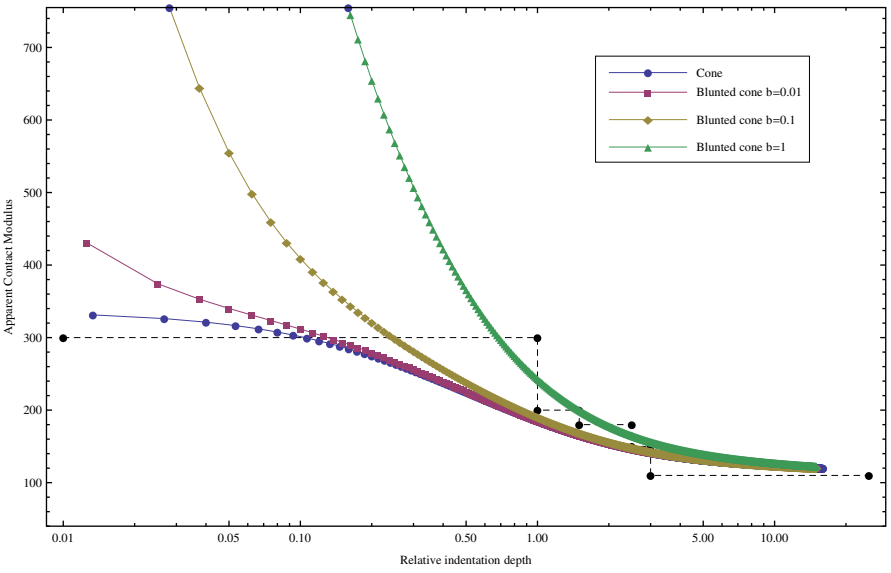

Fig. 7. The apparent contact modulus versus relative indentation depth for perfectly bonded bi-layer indented by a cone and with a blunted cone with blunt spot radii $b = 0.01, 0.1, 1$.

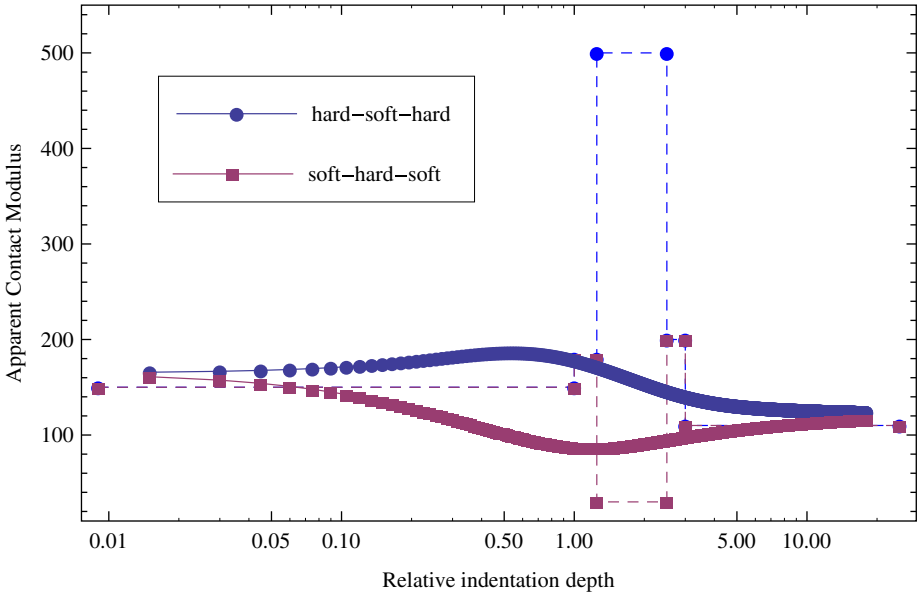

Fig. 8. Evolution of the apparent contact modulus with respect to the relative indentation depth for perfectly bonded 4-layer indented by a cone.

The complete numerical programming of the integration agorithm using the Mathematica as well as an example file are provided in the supplementary material (see files `MultiLayerIndentation.m` and `ExampleIndentation.nb` respectively).

4. Results and discussion

In a preliminary step, the accuracy and efficiency of the above computing method were verified by comparison of the results with some well-known analytical solutions for the indentation of the homogenous half-plane (Sneddon, 1965) and the indentation of a layer bonded to a dissimilar substrate (Korsunsky and Constantinescu, 2009; Li and Chou, 1997). The program was also used with an arbitrary number of layers with the same elastic properties resting on a similar and dissimilar elastic substrate.

The solution procedure was then applied for the indentation of a multilayered solid consisting of n dissimilar thin films on an elastic half-space, as shown in Fig. 1. Several indenter shapes were considered: flat punch, spherical cap, conical indenter and a blunted conical indenter (see Fig. 2). The corresponding functions $\delta(r)$ giving the shape and the functions $F(\tau)$ representing the right hand side of the Fredholm equation are reported in Table 1.

The Figs. 3–10 illustrate the evolution of the apparent contact modulus with respect to the relative indentation depth, i.e. the indenter penetration normalized by the thickness of the top layer film. The evolution of the apparent contact modulus obtained from the indentation result is represented with a continuous line, wether the evolution of the real Young's modulus is represented using a dashed line.

The first example considered is the indentation with a conical punch of a Al/SiC multilayer laminate deposed on Si (111) single-

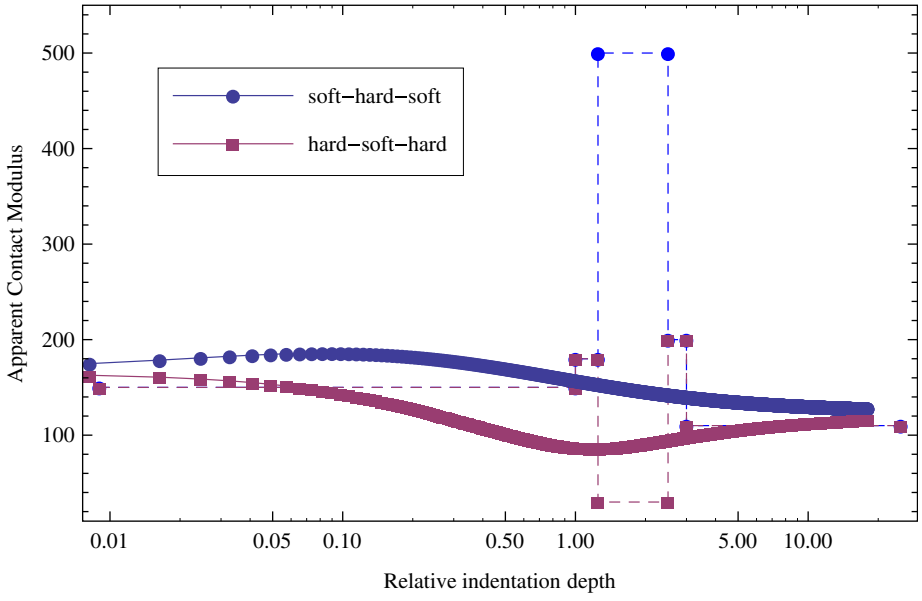

Fig. 9. The apparent contact modulus versus relative indentation depth for perfectly bonded 4-layer indented by a spherical punch.

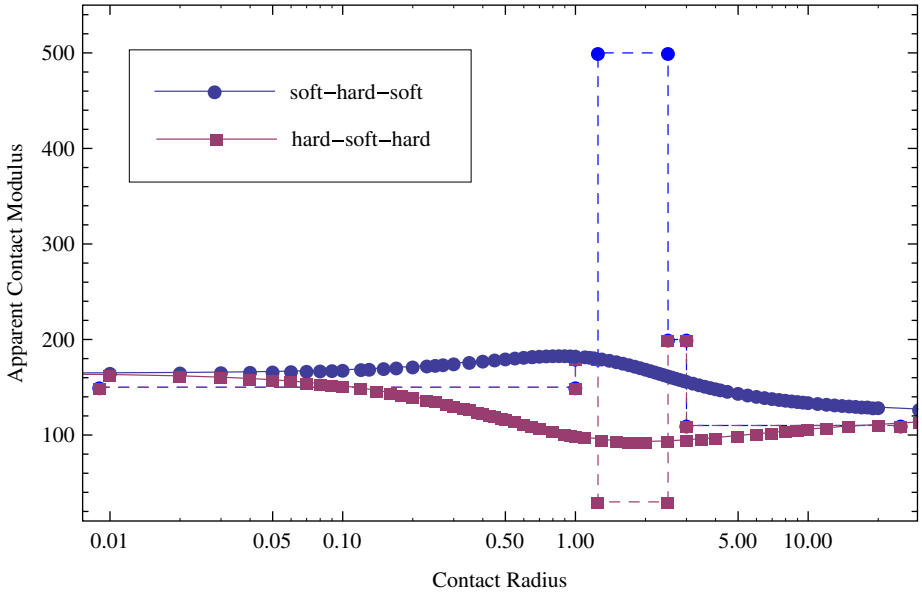

Fig. 10. The apparent contact modulus versus relative indentation depth for perfectly bonded 4-layer indented by a flat punch.

crystal substrate (Tang et al., 2009). The elastic properties are ($E_{Al} = 65$ GPa, $\nu_{Al} = 0.33$) for the Al film, ($E_{SiC} = 277$ GPa, $\nu_{Al} = 0.17$) for the SiC layer and ($E_f = 187$ GPa, $\nu_f = 0.28$) for the substrate. Fig. 3 shows the variation of the apparent contact modulus for a multilayer composite of n layers ($n \in \{1, 4, 7\}$), Al always being the top (first) layer.

Some features may be observed. For instance, we distinguish two limiting states: (i) for a very small prescribed displacement d, the apparent contact modulus approaches the plane strain modulus of the first layer; (ii) when the load is large enough, E^* approaches the modulus of the substrate. In the intermediate region, the contact radius increases with the applied load and the region of significant deformation gradually extends across the sub-layers and into the substrate. On can also remark that transition between the two limiting states is accelerated with the decreasing number of layers n, an intuitively anticipated effect.

Figs. 4–6 illustrate the variation of the apparent contact modulus for a perfectly bonded bi-layer indented by a conical, spherical and flat indenter respectively. Purely for the purposes of shorthand terminology, below we will use "hard" and "soft" to refer to "stiff" and "compliant" materials. Since the entire analytical treatment presented here concerns elastic processes, no plastic deformation is implied. A hard coating on a soft substrate and the reverse are considered with the following parameters: ($E_1 = 700$ GPa, $\nu_1 = 0.3$), ($E_2 = 200$GPa, $\nu_2 = 0.25$), ($E_f = 100$GPa, $\nu_f = 0.2$). Since the flat punch has a fixed contact radius that is independent of the indentation depth, the apparent contact modulus is constant for a given contact area. In the present work the contact radius was normalized by the thickness of first layer. As a consequence one can now plot the evolution of the apparent contact modulus versus the relative contact radius instead of the relative indentation depth. As for the other indentor shapes, it can be observed that the apparent contact modulus evolves from the modulus of the first layer for the small load d (small contact radii for flat punch) to the modulus of the substrate (under sufficiently large applied load and relative indentation depth). An inspection of the transition region in different figures allows to asses that the extent of this zone depends on the type of the indenter. Finite numerical accuracy causes the fluctuation of the computed contact modulus at high contact radii (see Fig. 6). This can be reduced using a greater number of integration points in the Gauss–Legendre quadrature.

Let us now consider the indentation of a multilayer with a blunted cone, which is closer to reality as perfectly sharp indenters do not exist. A simple inspection of the asymptotic expression of the function $F(\tau)$ in Table 1 for the blunted cone shows that for small contact zones, F is identical with that for a spherical indenter with radius $R = cot(\alpha)/b$, while for great value of the contact region F is close to the one created by a cone. In Fig. 7, we display the variation of contact modulus of a multilayer composed of 4 bonded films indented by a cone and several blunted cones with blunt spot radii $b \in \{0.01, 0.1, 1\}$. The elastic properties are listed in Table 2.

Noteworthy is the large overprediction of the apparent contact modulus induced by the use of blunted indenters for shallow indenter penetration. The figure clearly indicates a significant divergence between the results of the perfect sharp cone and blunted indenters even for very small degrees of blunting.

Let us now consider bilayers where a very compliant or a very stiff thin film is located between the substrate and the top layer.

Table 2
Elastic properties of a coating composed of 4 sub-layers over an elastic substrate indented by a conical and a blunted conical punch.

	Layer 1	Layer 2	Layer 3	Layer 4	Substrate
E (GPa)	300	200	180	150	110
ν	0.33	0.28	0.25	0.2	0.17

Table 3
Young modulus and Poisson's ratio for the the S-H-S and H-S-H multilayers configurations.

		Film 1	Film 2	Film 3	Film 4	Substrate
H–S–H	E (GPa)	150	180	30	200	110
	ν	0.3	0.2	0.25	0.2	0.3
S–H–S	E (GPa)	150	180	500	200	110
	ν	0.3	0.2	0.25	0.2	0.3

The first configuration is denoted by S–H–S and the second one by H–S–H. Figs. 8–10 display the results of the indentation of multilayered solid containing 4 bonded films by a spherical, conical and flat rigid stamps, respectively. The elastic properties are reported in Table 3.

It can be seen that the values of the contact modulus are evolving as expected from that of the first layer for very small depths to the value of substrate's modulus for large indentations depth. In the transition zone, the curves show peak values of the apparent contact modulus for S–H–S configuration and a minimum for the H–S–H case. The results further show that the magnitude of the extremum values and the extent of the transition zone depend on the indenter shape.

5. Conclusion

The present paper introduced a semi-analytical solution procedure of the axisymmetric and frictionless indentation problem of a multi-layered half-space. A transfer matrix approach was used in order to capture the boundary conditions between the elastic solids from the top sub-layer to the substrate. The problem was then reduced to a Fredholm integral equation of the second kind defined on the contact patch, and stress and displacement continuity condition. The solution was implemented in *Mathematica*, giving a fast and efficient symbolic/numerical code (`TransferMatrix.nb`, `MultiLayerIndentation.m`, `ExampleIndentation.nb`) provided with the paper.

The method of solution can also be applied for a large wide material combinations, for arbitrary thickness of the sub-layers spanning from nano to macro scale, and for a large spectrum of indentation loads exerted by different kinds of indenters.

A common feature of all the above examples is that, for very shallow indentation, the apparent contact modulus approaches the value of the top sub-layer, while for very large indentation loads, it converges toward the substrate's modulus. The extent of the transition zone between these two asymptotic cases depends on the indenter shape and the elastic properties of the layers.

Acknowledgement

The first draft of the paper was written during the stay of OP and AC at Tokyo Institute of Technology. They would like to thank Professor Kikuo Kishimoto for the excellent time spend in his laboratory and the fruitfull discussions.

Appendix A. Supplementary data

Supplementary data associated with this article can be found, in the online version, at http://dx.doi.org/10.1016/j.ijsolstr.2013.04.017.

References

Bahar, L.Y., 1972. Transfer matrix approach to layered system. J. Eng. Mech. Div., ASCE 98, 1159–1172.
Choi, I.S., Dao, M., Suresh, S., 2008a. Mechanics of indentation of plastically graded materials-I: analysis. J. Mech. Phys. Solids 56, 157–171.

Choi, I.S., Detora, A.J., Schwaigerb, R., Daoa, M., Schuha, C.A., Suresh, S., 2008b. Mechanics of indentation of plastically graded materials-II: experiments on nanocrystalline alloys with grain size gradients. J. Mech. Phys. Solids 56, 172–183.

Constantinescu, A., Korsunsky, A.M., 2007. Elasticity with Mathematica. Cambridge University Press.

Dao, M., Chollacoop, N., Vliet, K.J.V., Venkatesh, T.A., Suresh, S., 2001. Computational modeling of the forward and reverse problems in instrumented sharp indentation. Acta Mater. 49, 3899–3918.

Delafargue, A., Ulm, F.J., 2004. Explicit approximations of the indentation modulus of elastically orthotropic solids for conical indenters. Int. J. Solids Struct. 41, 7351–7360.

Fretigny, C., Chateauminois, A., 2007. Solution for the elastic field in a layered medium under axisymmetric contact loading. J. Phys. D: Appl. Phys. 40, 5418–5426.

Giannakopoulos, A.E., Suresh, S., 1997. Indentation of solids with gradients in elastic properties: Part I. Point force. Int. J. Solids Struct. 34, 2357–2392.

Giannakopoulos, A.E., Suresh, S., 1997. Indentation of solids with gradients in elastic properties: Part II. Axisymmetric indentors. Int. J. Solids Struct. 34, 2393–2428.

Ke, L.L., Wang, Y.S., 2006. Two-dimensional contact mechanics of functionally graded materials with arbitrary spatial variations of material properties. Int. J. Solids Struct. 43, 5779–5798.

Korsunsky, A.M., Constantinescu, A., 2009. The influence of indenter bluntness on the apparent contact stiffness of thin coatings. Thin Solid Films 517, 4835–4844.

Lebedev, N.N., Uflyand, I.S., 1958. Axisymmetric contact problem for an elastic layer. PMM 22, 320–326.

Li, J., Chou, T.W., 1997. Elastic field of a thin-film/substrate system under an axisymmetric loading. Int. J. Solid Struct. 34, 4463–4478.

Oliver, W.C., Pharr, G.M., 1992. An improved technique for determining hardness and elastic modulus using load and displacement sensing instruments. J. Mater. Res. 7, 1564–1583.

Oliver, W.C., Pharr, G.M., 2004. Measurement of hardness and elastic modulus by instrumented indentation: advances in understanding and refinements to methodology. J. Mater. Res. 19, 3–19.

Sneddon, I.N., 1965. The relation between load and penetration in the axissymetric Bousinesq problem for a punch of arbitrary profile. Int. J. Eng. Sci. 3, 47–57.

Soutas-Little Robert, W., 1999. Elasticity. Dover Publications.

Solomon, L., 1968. Elasticité Linéaire. Masson, Paris.

Swadener, J.G., Pharr, G.M., 2001. Indentation modulus of elastically anisotropic half-spaces by cones and parabola of revolution. Philos. Mag. A 81, 447–466.

Tang, G., Singh, D.R.P., Shen, Y.L., Chawla, N., 2008. Analysis of indentation-derived effective elastic modulus of metal-ceramic multilayers. Int. J. Mech. Mater. Design 4, 391–398.

Tang, G., Singh, D.R.P., Shen, Y.L., Chawla, N., 2009. Elastic properties of metal–ceramic nanolaminates measured by nanoindentation. Mater. Sci. Eng. A 502, 79–84.

Vlassak, J.J., Nix, W.D., 1994. Measuring the elastic properties of anisotropic materials by means of indentation experiments. J. Mech. Phys. Solids 42, 1223–1245.

Vlassak, J.J., Ciavarella, M., Barber, J.R., Wang, X., 2003. The indentation modulus of elastically anisotropic materials for indenters of arbitrary shape. J. Mech. Phys. Solids 51, 1701–1721.

Wolfram. Mathematica. <http://www.wolfram.com>

Wang, J., Fang, S., Chen, L., 2002. The state vector methods for space axisymmetric problems in multilayered piezoelectric media. Int. J. Solids Struct. 39, 3959–3970.

Yu, H.Y., Sanday, S.C., Rath, B.B., 1990. The effect of substrate on the elastic properties of films determined by the indentation test – Axisymmetric Boussinesq problem. J. Mech. Phys. Solids 38 (6), 745–764.

Yue, Z.Q., Yin, J.H., 1998. Backward transfer-matrix method for elastic analysis of layered solids with imperfect bonding. J. Elasticity 50, 109–128.